arXiv:1211.1031v2 [astro-ph.EP] 4 Jun 2013

KELT-3B: A HOT JUPITER TRANSITING A $V = 9.8$ LATE-F STAR

JOSHUA PEPPER[1,2], ROBERT J. SIVERD[2], THOMAS G. BEATTY[3], B. SCOTT GAUDI[3], KEIVAN G. STASSUN[2,4], JASON EASTMAN[5,6], KAREN COLLINS[7], DAVID W. LATHAM[8], ALLYSON BIERYLA[8], LARS A. BUCHHAVE[9,10], ERIC L. N. JENSEN[11], MARK MANNER[12], KALOYAN PENEV[13], JUSTIN R. CREPP[14], PHILLIP A. CARGILE[2], SAURAV DHITAL[2,15], MICHAEL L. CALKINS[8], GILBERT A. ESQUERDO[8], PERRY BERLIND[8], BENJAMIN J. FULTON[5,16], RACHEL STREET[5], BO MA[17], JIAN GE[17], JI WANG[18], QINGQING MAO[2], ALEXANDER J. W. RICHERT[19], ANDREW GOULD[3,20], DARREN L. DEPOY[21], JOHN F. KIELKOPF[7], JENNIFER L. MARSHALL[21], RICHARD W. POGGE[3,20], ROBERT P. STEFANIK[8], MARK TRUEBLOOD[22], PATRICIA TRUEBLOOD[22]
Draft version June 6, 2013

ABSTRACT

We report the discovery of KELT-3b, a moderately inflated transiting hot Jupiter with a mass of $1.477^{+0.066}_{-0.067} M_J$, and radius of $1.345 \pm 0.072 R_J$, with an orbital period of 2.7033904 ± 0.000010 days. The host star, KELT-3, is a $V = 9.8$ late F star with $M_* = 1.278^{+0.063}_{-0.061} M_\odot$, $R_* = 1.472^{+0.065}_{-0.067} R_\odot$, $T_{\rm eff} = 6306^{+50}_{-49}$ K, log(g) = $4.209^{+0.033}_{-0.031}$, and [Fe/H] = $0.044^{+0.080}_{-0.082}$, and has a likely proper motion companion. KELT-3b is the third transiting exoplanet discovered by the KELT survey, and is orbiting one of the 20 brightest known transiting planet host stars, making it a promising candidate for detailed characterization studies. Although we infer that KELT-3 is significantly evolved, a preliminary analysis of the stellar and orbital evolution of the system suggests that the planet has likely always received a level of incident flux above the empirically-identified threshold for radius inflation suggested by Demory & Seager (2011).

Subject headings:

1. INTRODUCTION

Transiting extrasolar planets are the best laboratories for studying the individual properties of exoplanets, providing clues about planetary formation and evolution. Informa-

[1] Department of Physics, Lehigh University, Bethlehem, PA 18015, USA
[2] Department of Physics and Astronomy, Vanderbilt University, Nashville, TN 37235, USA
[3] Department of Astronomy, The Ohio State University, Columbus, OH 43210, USA
[4] Department of Physics, Fisk University, Nashville, TN 37208, USA
[5] Las Cumbres Observatory Global Telescope Network, Santa Barbara, CA 93117, USA
[6] Department of Physics Broida Hall, University of California, Santa Barbara, CA 93106, USA
[7] Department of Physics & Astronomy, University of Louisville, Louisville, KY 40292, USA
[8] Harvard-Smithsonian Center for Astrophysics, Cambridge, MA 02138, USA
[9] Niels Bohr Institute, University of Copenhagen, 21S00 Copenhagen, Denmark
[10] Centre for Star and Planet Formation, Natural History Museum of Denmark, University of Copenhagen, DK-1350 Copenhagen, Denmark
[11] Department of Physics and Astronomy, Swarthmore College, Swarthmore, PA 19081, USA
[12] Spot Observatory, Nunnelly, TN 37137, USA
[13] Department of Astrophysical Sciences, Princeton University, Peyton Hall, Princeton, NJ 08544, USA
[14] Department of Physics, University of Notre Dame, Notre Dame, IN 46556, USA
[15] Department of Astronomy, Boston University, 725 Commonwealth Avenue, Boston, MA 02215, USA
[16] Institute for Astronomy, University of Hawaii, Honolulu, HI 96822, USA
[17] Department of Astronomy, University of Florida, Gainesville, FL 32611, USA
[18] Department of Astronomy, Yale University, New Haven, CT 06511 USA
[19] Department of Astronomy and Astrophysics, Pennsylvania State University, University Park, PA 16802, USA
[20] Center for Cosmology and Astroparticle Physics, The Ohio State University, OH 43210, USA
[21] Department of Physics & Astronomy, Texas A&M University, College Station, TX 77843, USA
[22] Winer Observatory, Sonoita, AZ 85637, USA

tion about planetary mass, radius, atmosphere, and spin-orbit alignment can most easily be gathered from transiting exoplanets that orbit bright stars, since the greater flux from such stars enables faster, cheaper, and more precise follow-up observations.

Several ground-based transit surveys (TrES, Alonso et al. (2004); XO, McCullough et al. (2006); HATNet, Bakos et al. (2007); SuperWASP, Collier Cameron et al. (2007a); QES, Alsubai et al. (2011)) have been conducted, some of which are still ongoing, and have produced a large number of exoplanet discoveries. SuperWASP and HATNet have been especially productive, with each survey discovering dozens of new transiting planets. The CoRoT (Baglin 2003) and Kepler (Borucki et al. 2010) space-based missions have also made numerous exoplanet discoveries, and have expanded the parameter space probed for transiting planets, finding those with both very long periods and much smaller radii.

The Kilodegree Extremely Little Telescope (KELT) transit survey is designed to find transiting planets around bright stars. The KELT-North telescope (Pepper et al. 2007) has a small aperture and wide field of view ($26° \times 26°$) to observe the entire sky between declinations 19°N and 45°N, covering approximately 40% of the northern sky. The aperture, optical system, and exposure time for KELT-North are configured to obtain better than 1% RMS photometry for stars with $8 < V < 10$. That magnitude range represents the brightness gap between comprehensive RV surveys and most other transit surveys. Specifically, while both SuperWASP and HATNet have been tremendously successful at discovering transiting exoplanets, the vast majority of their published discoveries (90% and 93%, respectively) are fainter than $V = 10$. On the other hand, RV surveys start to become incomplete for stars fainter than $V \sim 8$ (Wright et al. 2012).

The KELT-North survey has been operating since 2006, and we have been vetting transit candidates since April 2011. The first two KELT transit discoveries demonstrate the scientific potential of this effort. KELT-1b (Siverd et al. 2012) is a

$27M_J$ brown dwarf transiting a V=10.7 star. KELT-1 is the brightest star known to host a transiting brown dwarf. KELT-2Ab (Beatty et al. 2012) is a transiting hot Jupiter orbiting a V=8.77 star. KELT-2A, the brighter of two stars in a visual binary, is the ninth-brightest star known to harbor a transiting planet and the third-brightest discovered to date by a ground-based transit survey. In this paper we describe the discovery and characterization of a hot Jupiter transiting the bright V=9.8 star TYC 2996-683-1.

2. DISCOVERY AND FOLLOW-UP OBSERVATIONS

The KELT survey has an established process for reducing KELT survey data, extracting light curves, identifying potential transiting planets, and performing follow-up observations. We provide a brief summary of the KELT reductions in §2.1; for more details, see §2 of Siverd et al. (2012).

2.1. KELT Observations and Photometry

KELT-3 is in KELT-North survey field 06, which is centered on (α=09h:46m:48s, δ=+31d:44m:37s; J2000). We monitored field 06 from October 27, 2006, to April 1, 2011, collecting a total of 6,619 observations. We reduced the raw survey data using a custom implementation of the ISIS image subtraction package (Alard & Lupton 1998; Alard 2000), combined with point-spread fitting photometry using DAOPHOT (Stetson 1987). Using proper motions from the Tycho-2 catalog (Høg et al. 2000) and a reduced proper motion cut (Gould & Morgan 2003) based on Collier Cameron et al. (2007b), we selected likely dwarf and subgiant stars within the field for further post-processing and analysis. We applied the trend filtering algorithm (TFA; Kovács et al. 2005) to each remaining light curve to remove systematic noise, followed by a search for transit signals using the box-fitting least squares algorithm (BLS; Kovács et al. 2002). For both TFA and BLS we used the versions found in the VARTOOLS package (Hartman et al. 2008).

One of the candidates from field 06 was star BD+41 2024 / TYC 2996-683-1 / 2MASS J09543439+4023170, located at (α=09h:54m:34.388s, δ=+40d:23m:16.98s; J2000). The star (henceforth KELT-3) has Tycho magnitudes $B_T = 10.397 \pm 0.032$ and $V_T = 9.873 \pm 0.029$ (Høg et al. 2000) (Johnson magnitudes $B = 10.27$ and $V = 9.82$), and passed our initial selection cuts. The discovery light curve of KELT-3 is shown in Figure 1. We observed a transit-like feature at a period of 2.70339 days, with a depth of about 10 mmag.

KELT-3 has a faint ($r = 13.3$) nearby stellar neighbor about 3.7 arcseconds to the northeast, SDSS7 J095434.58+402319.6 (SDSS-DR7; Adelman-McCarthy & et al. 2009). The presence of this object (henceforth SDSS7J095434) complicates some of our analysis, which we address in §3.5.

2.2. Radial-Velocity Observations

After KELT-3 was selected as a candidate, we conducted radial-velocity (RV) observations to identify possible false-positive signatures and to determine the RV orbit. We obtained data using the Tillinghast Reflector Echelle Spectrograph[23] (TRES; Fűrész 2008), on the 1.5m Tillinghast Reflector at the Fred L. Whipple Observatory (FLWO) at Mt. Hopkins, AZ. We observed KELT-3 sixteen times with TRES over two months, from UT February 26, 2012, to UT May 2,

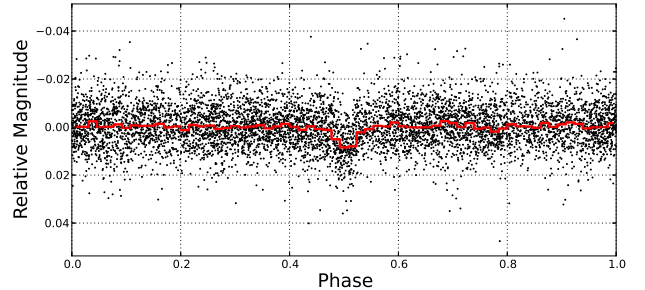[23] http://tdc-www.harvard.edu/instruments/tres/

FIG. 1.— Discovery light curve of KELT-3b from the KELT-North telescope. The light curve contains 6,619 observations spanning 4.4 years, phase-folded to the orbital period of 2.70339 days. The red line represents the same data binned at 1-hour intervals in phase.

2012. The spectra had a resolving power of R=44,000, and were extracted following the procedures described by Buchhave et al. (2010).

We also observed KELT-3 with the FIbre-fed Echelle Spectrograph (FIES) on the 2.5 m Nordic Optical Telescope (NOT) in La Palma, Spain (Djupvik & Andersen 2010). We acquired 5 FIES spectra between 13 and 17 March 2012 with the high–resolution fiber (1.″3 projected diameter) with resolving power of R $\approx$ 67,000, and wavelength coverage of $\sim$3600-7400 Å. We used the wavelength range from approximately 4000-6100 Å to determine the radial velocities. The exposure times ranged from 7 to 15 minutes, yielding a SNR from 31 to 52 pixel^{-1} (SNR of 49 to 83 per resolution element) in the wavelength region containing the Mgb triplet. The procedures used to reduce the FIES spectra and extract the radial velocities are those described in Buchhave et al. (2010) and the spectral classification of the FIES spectra is described in Buchhave et al. (2012).

We also obtained follow-up RV measurements from the 2.1m telescope at Kitt Peak National Observatory using the R=30,000 Direct Echelle Mode of the EXPERT spectrograph (Ge et al. 2010). Four EXPERT RV measurements were acquired between 20 and 24 January 2013. The exposure time for each observation ranged from 25 to 40 minutess, yielding a SNR $\sim$ 80 per pixel around 5400 Å. Spectra were reduced using an IDL pipeline modified from an early version described in Wang (2012). Frames were trimmed, bias subtracted, flat-field corrected, aperture-traced and extracted. All the frames were combined together to serve as a star template. Radial velocities were derived via cross-correlation with this template from the wavelength range $4900-6300$ Å.

Table 1 lists all RV data for KELT-3, and Figure 2 shows the RV data phased to the orbit fit, along with the residuals to the model fit. All RV observations were conducted with fibers with diameters smaller than 2.6 arcseconds, so there is no expected significant contamination from SDSS7J095434, which is about 3.7 arcseconds away. We compute the bisector spans for the TRES and FIES observations. We find the RMS of the bisector spans to be 13.2 m s^{-1}, which is significantly lower than the RV semi-amplitude of 182.0 m s^{-1}. The absence of a trend and low RMS of the bisector spans in phase suggests that the measured RV variations are due to real RV variations in the target star. Although we do not have bisector spans calculated for the EXPERT data, those constitute only 4/25 RV points, so the bisector results from the other instruments should be sufficient to allay any concerns about the origin of

TABLE 1
RV Observations of KELT-3

BJD (TDB)	RV (m s^{-1})	RV error[a] (m s^{-1})	Source
2455983.672916	-319	25	TRES
2455990.777987	-66	14	TRES
2456000.473809	-31	27	FIES
2456001.465355	103	20	FIES
2456002.514673	-259	20	FIES
2456003.552533	90	16	FIES
2456004.432251	0	16	FIES
2456018.656206	-324	14	TRES
2456019.709404	4	19	TRES
2456020.710562[b]	-125	18	TRES
2456021.776310	-282	10	TRES
2456022.786222	0	10	TRES
2456023.806566	-293	13	TRES
2456024.741118	-173	19	TRES
2456025.668112	2	18	TRES
2456026.816586	-334	14	TRES
2456029.644415	-357	13	TRES
2456033.837821	21	20	TRES
2456045.694187	-333	15	TRES
2456048.634878	-331	23	TRES
2456049.760849	22	21	TRES
2456311.939539	7	29	EXPERT
2456313.983608	-243	23	EXPERT
2456314.940516	12	24	EXPERT
2456315.965642	-320	25	EXPERT

[a]Unrescaled measurement errors.

[b]This observation occured during transit and was excluded from the EXO-FAST analysis in §3.5.
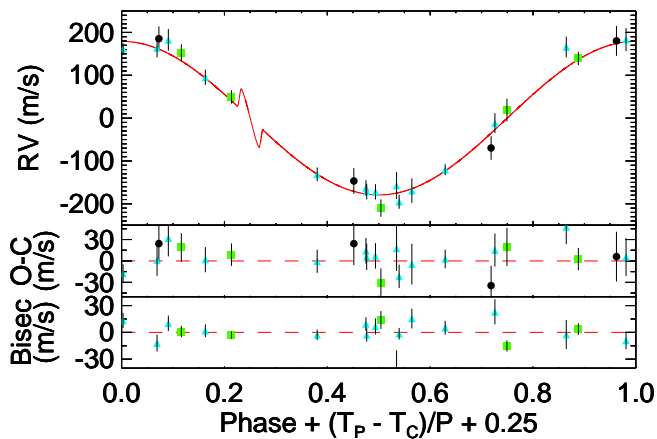

Fig. 2.— Radial velocity measurements of KELT-3. *Top panel:* RV observations phased to our best orbital model with eccentricity fixed to zero and with no linear trend, shown in red. TRES observations are shown as blue triangles, FIES observations are green squares, EXPERT observations are black circles, and the error bars are scaled according to the method described in §3.5. The RV observation taken during transit is not plotted. The predicted Rossiter-McLaughlin effect in the model shown incorporates an assumption that $\lambda = 0$ (i.e. that the projected spin-obit alignment of the system is 0 degrees). *Middle panel:* Residuals of the RV observations to our circular orbital fit. *Bottom panel:* Bisector span of the TRES and FIES observations as a function of phase.

the RV signal.

2.3. *Follow-up Time-Series Photometry*

We acquired follow-up time-series photometry of KELT-3 to check for other types of false positives and to better determine the transit shape. To schedule followup photometry,

we used the Tapir software package[24]. We obtained eight partial or full transits in multiple bands between March and June 2012. For all instruments except FTN, the faint neighbor SDSS7J095434 was included in the photometric aperture, and so the resultant light curves include both KELT-3 and SDSS7J095434. Figure 3 shows all the follow-up light curves assembled. We find that the R_P/R_* ratio is the same to within the measurement errors in all light curves, which include observations in the g, r, i, and Pan-Starrs-Z filters[25], helping to rule out false positives due to blended eclipsing binaries.

We observed two transits of KELT-3 at Swarthmore College's Peter van de Kamp Observatory. The observatory uses a 0.6m RCOS telescope with an Apogee U16M 4K × 4K CCD, giving a 26' × 26' field of view. Using 2 × 2 binning, it has 0.76 arcseconds pixel^{-1}. On UT 2012-03-17 we obtained a partial transit including egress in r. On UT 2012-04-13 we observed an entire transit in g.

We observed two transits of KELT-3 at Moore Observatory, operated by the University of Louisville. We used the 0.6m RCOS telescope with an Apogee U16M 4K × 4K CCD, giving a 26' × 26' field of view and 0.39 arcseconds pixel^{-1}. The data were calibrated with the AstroImageJ package (Collins, et al., in preparation). On UT 2012-04-02 we obtained a full transit in i, although observing conditions created some interruptions in the data. On UT 2012-06-07 we obtained a nearly-full transit in r.

We observed two transits with Faulkes Telescope North (FTN), operated by Las Cumbres Observatory Global Telescope (LCOGT). FTN is a 2.0m telescope with a 4K × 4K Spectral camera, and we bin the transit observations in 2 × 2 mode. On UT 2012-04-02 we obtained a partial transit in Pan-Starrs-Z, which includes most of the in-transit phase plus the full egress. On UT 2012-04-12 we obtained a full transit in Pan-Starrs-Z. Both observations were able to resolve KELT-3 from SDSS7J095434.

We observed a full transit from Byrne Observatory at Sedgwick (BOS), also operated by LCOGT. BOS is an 0.8m telescope with an 3K × 2K SBIG STL-6303E camera with 0.572 arcseconds pixel^{-1} and a 14.7' × 9.8' field of view. On UT 2012-04-03 we obtained a full transit in g, using 2 × 2 binning.

We observed a full transit in i on UT 2012-04-03 with KeplerCam on the 1.2m telescope at FLWO. KeplerCam has a single 4K × 4K Fairchild CCD with 0.366 arcseconds pixel^{-1}, and a field of view of 23.1' × 23.1'. The data were reduced using procedures outlined in Carter et al. (2011), which uses standard IDL routines.

2.4. *Single-epoch Multiband Photometry of SDSS7J095434*

In an effort to better characterize the relative colors and magnitudes of KELT-3 and SDSS7J095434, we observed the stars with FTN on UT 2012-04-02 in good conditions in the g, r, i and Pan-Starrs-Z filters. We find that the neighbor has $g = 14.05 \pm 0.23$, $r = 13.35 \pm 0.17$, $i = 12.85 \pm 0.17$, and $PS-Z = 12.48 \pm 0.19$.

2.5. *Adaptive Optics Observations*

[24] https://github.com/elnjensen/Tapir, submitted to the Astrophysics Source Code Library

[25] In all references to SDSS filters in this paper, we use the unprimed notation, to denote generic SDSS-like filters, which in practice are often labeled with the primed notation.
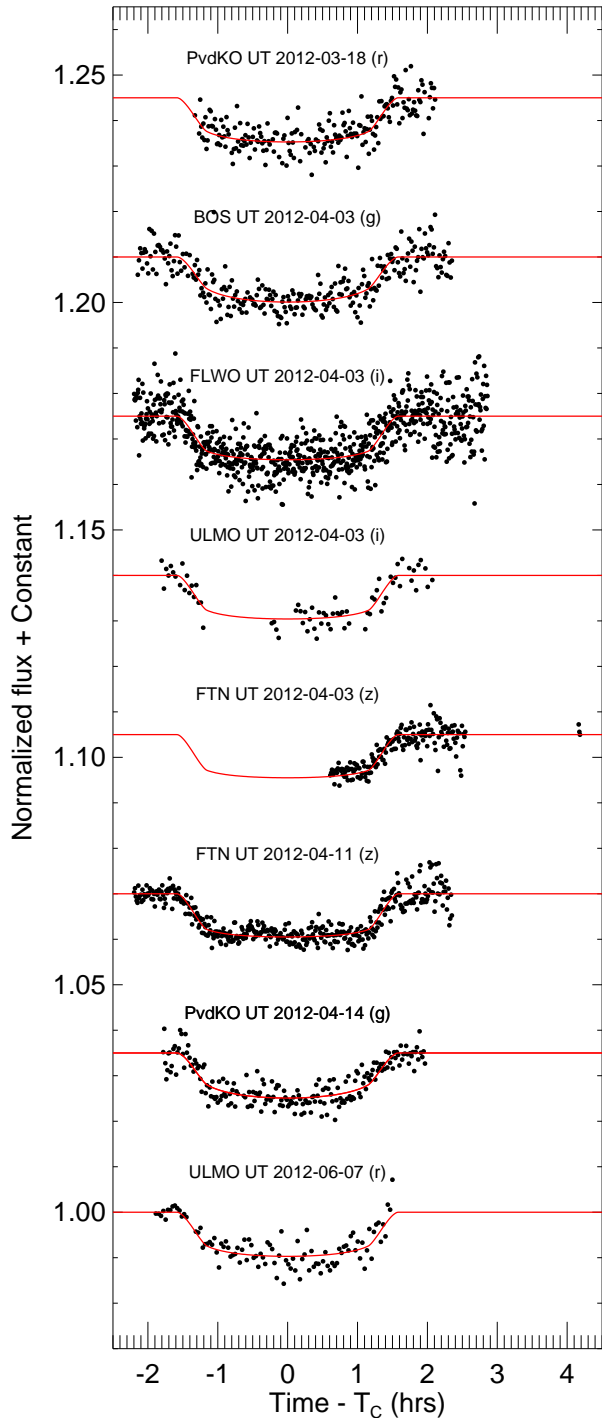
FIG. 3.— Follow-up transit photometry of KELT-3. The red overplotted lines are the best fit transit model. The labels are as follows: PvdKO - Peter van de Kamp Observatory (Swarthmore); ULMO - University of Louisville Moore Observatory; FTN - Faulkes Telescope North (LCOGT); BOS - Byrne Observatory at Sedgwick (LCOGT); FLWO - KeplerCam at Fred L. Whipple Observatory.

In order to better assess the nature of SDSS7J095434 and search for any other faint neighbors, we obtained adaptive optics images using NIRC2 (instrument PI: Keith Matthews) at
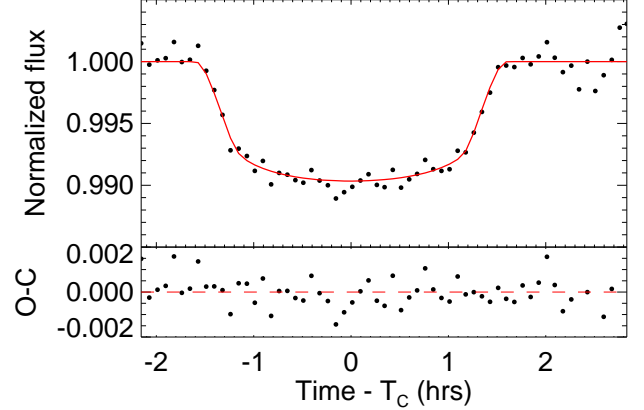

FIG. 4.— *Top panel:* All follow-up light curves from Figure 3, combined and binned in 5 minute intervals. This light curve is not used for analysis, but is shown in order to illustrate the statistical power and behavior of the combined light curve dataset. The red curve shows the six transit models for each of the individual fits combined and binned in 5 minute intervals the same way as the data, with the model points connected. *Bottom panel:* The residuals of the binned light curve from the binned model in the top panel.

Keck on UT 2012-05-07. Our observations consist of dithered frames taken with the *K'* and *J* filters. We used the narrow camera setting to provide fine spatial sampling of the stellar point-spread function, and used KELT-3 as its own on-axis natural guide star. The total on-source integration time was 16.3 seconds in each bandpass. The resulting *K'* image is shown in Figure 5.

We find no other faint neighbors in the immediate vicinity of KELT-3. Specifically, we can exclude additional companions beyond a distance of 0.5 arcseconds from KELT-3 down to a magnitude difference of 6.5 magnitudes at 10–σ confidence. The magnitude differences between KELT-3 and SDSS7J095434 are $\Delta J = 3.001 \pm 0.019$ mag, and $\Delta K' = 2.436 \pm 0.014$ mag. The angular separation between the stars is 3724 ± 1 mas and the position angle of SDSS7J095434 is 42.00 ± 0.03 degrees, measured east of North.

3. SYSTEM PARAMETERS AND FITS

3.1. *Spectroscopic Analysis*

We use both the TRES and FIES spectra to derive the stellar properties of KELT-3. Using the Spectral Parameter Classification (SPC) procedure (Buchhave et al. 2012), we obtained stellar parameters from the average of all 16 TRES spectra, and separately from all 5 FIES spectra. Since each dataset yielded similar results, we combined the data from all 21 spectra, which yielded from SPC the following results: $T_{\rm eff} = 6308 \pm 50$ K, $\log(g) = 4.23 \pm 0.10$, $[m/H] = 0.04 \pm 0.08$, and $V_{\rm rot} = 10.2 \pm 0.5$ km s^{-1}, giving the star an inferred spectral type of F7V. Based on those results, we are able to calculate the stellar mass and radius from the relations of Torres et al. (2010). In this case, we used [m/H] as a substitute for [Fe/H], but we do not believe that the difference should affect the results. We find that $M_* = 1.28 \pm 0.12 M_\odot$, and $R_* = 1.44 \pm 0.21 R_\odot$.

3.2. *SED Analysis*

We construct an empirical spectral energy distribution (SED) of KELT-3 using the FUV and NUV bandpasses from GALEX (Martin et al. 2005), the B_T and V_T colors from the Tycho-2 catalog (Høg et al. 2000), near-infrared (NIR) fluxes
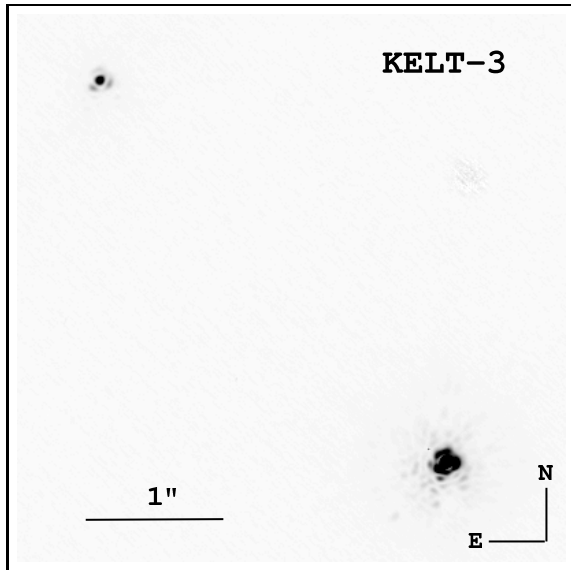
FIG. 5.— Keck adaptive optics image of KELT-3 taken with NIRC2 in the K' filter. KELT-3 is in the lower right corner of the panel, while the nearby star SDSS7J095434 is in the upper left, located 3.742 ± 0.001 arcseconds to the north east.
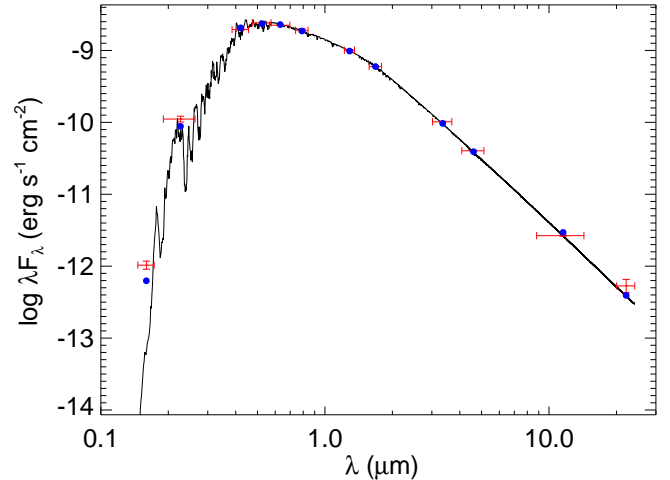

FIG. 6.— Measured and best-fit SED for KELT-3 from UV through NIR. The red errorbars indicate measurements of the flux of KELT-3 in UV, optical, and NIR passbands listed in Table 2. The vertical errorbars are the $1-\sigma$ photometric uncertainties, whereas the horizontal errorbars are the effective widths of the passbands. The solid curve is the best-fit theoretical SED from the NextGen models of Hauschildt et al. (1999), assuming stellar parameters $T_{\rm eff}$, log(g) and [Fe/H] fixed at the values in Table 3 from the circular fit, with A_V and d allowed to vary. The blue dots are the predicted passband-integrated fluxes of the best-fit theoretical SED corresponding to our observed photometric bands.
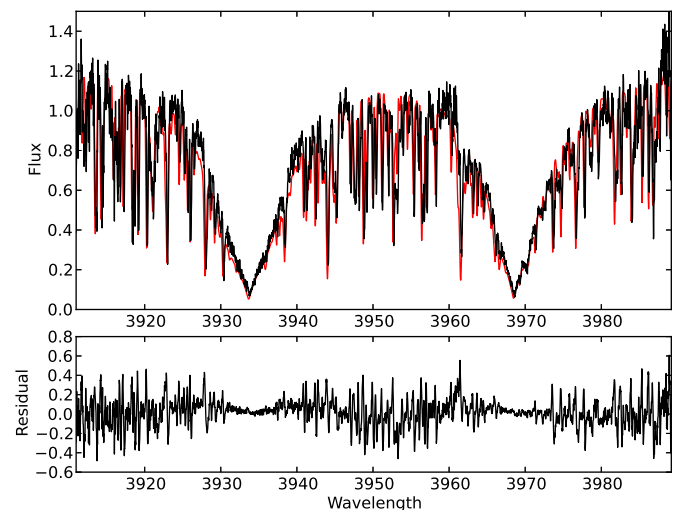
in the J and H passbands from the 2MASS Point Source Catalog (Cutri et al. 2003; Skrutskie et al. 2006), and near- and mid-IR fluxes in the four WISE passbands (Wright et al. 2010), to derive the SED shown in Figure 6. We fit this SED to NextGen models from Hauschildt et al. (1999) by fixing the values of $T_{\rm eff}$, log(g) and [Fe/H] inferred from the global fit to the light curve and RV data as described in §3.5 and listed in Table 3 for the circular orbit, and then finding the values of the visual extinction A_V and distance d that minimize χ^2. We find $A_V = 0.02 \pm 0.02$ and $d = 178 \pm 16$ pc. We note that the quoted statistical uncertainties on A_V and d are likely to be underestimated because we have not accounted for the uncertainties in values of $T_{\rm eff}$, log(g) and [Fe/H] used to derive the model SED. Furthermore, it is likely that alternate model atmospheres would predict somewhat different SEDs and thus values of the extinction and distance.

We also evaluate the motion of KELT-3 through the Galaxy to place it among standard stellar populations. The TRES RV observations show that it has a bulk radial velocity of $+27.9 \pm 0.2$ km s^{-1}. Combining that with the distance and proper motion information from the NOMAD catalog (Zacharias et al. 2004), we find that KELT-3 has 3-space motion of U, V, W (where positive U is in the direction of the Galactic center) of $-25.6 \pm 1.6, -11.0 \pm 2.2, 14.6 \pm 1.3$, all in units of km s^{-1}, making it a thin disk star.

We checked the signatures of chromospheric activity in KELT-3 from the spectroscopic observations, but we find no visible emission in the cores of the Ca-II H and K absorption lines, suggesting an essentially inactive star. That analysis is shown in Figure 7. The observed spectrum is compared with a synthetic spectrum generated using SME (Valenti & Piskunov 1996; Valenti & Fischer 2005) based on the stellar parameters from §3.5, model atmospheres from Kurucz (1992), and the line list from Kupka et al. (2000).

3.3. Evolutionary Analysis

In Figure 8 we plot the predicted evolutionary track of KELT-3 on a theoretical HR diagram (log(g) vs. $T_{\rm eff}$), from

FIG. 7.— No evidence is seen for chromospheric activity in the spectrum of KELT-3. *Upper Panel*: The black curve shows the combined spectra for KELT-3 from the FIES observations, while the red line shows a synthetic spectrum generated using SME. The spectral range encompasses the Ca H and Ca K absorbtion lines, and no emission is seen in the core from either spectrum, consistent with no signs of chromospheric activity in KELT-3. *Lower Panel*: Residuals between the observed and synthetic spectra. The scatter in this plot mostly comes from missing line information in the line list for the synthetic spectrum and not noise in either spectrum. The noise level can be seen in the central parts of the Ca lines.
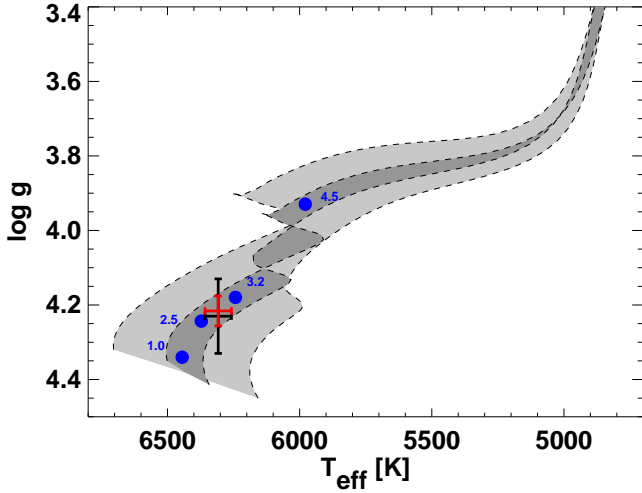
FIG. 8.— Theoretical HR diagram based on Yonsei-Yale stellar evolution models (Demarque et al. 2004). The gray swaths represent the evolutionary track for the best-fit values of the mass and metallicity of the host star from the circular joint fit described in §3.5, $M_* = 1.282^{+0.062}_{-0.060} M_\odot$ and [Fe/H] $= 0.048^{+0.079}_{-0.081}$ (dark shaded), and from the spectroscopic constraints alone (light shaded). The tracks for the extreme range of the $1-\sigma$ uncertainties on M_* and [Fe/H] from the spectroscopic data only and from the final analysis are shown as dashed lines bracketing the light and dark gray swaths, respectively. The red cross shows the best-fit $T_{\rm eff} = 6304 \pm 49$K and log(g) $= 4.204^{+0.031}_{-0.029}$ from the final EXOFAST analysis. The black cross shows the inferred $T_{\rm eff}$ and log(g) from the spectroscopic analysis alone. The blue dots represent the location of the star for various ages in Gyr. The host star is slightly evolved with a probable age of 3.0 ± 0.02 Gyr.

the Yonsei-Yale stellar models (Demarque et al. 2004). Here we have used the stellar mass and metallicity derived from the global circular orbit fit (§3.5 and Table 3). We also show evolutionary tracks for masses corresponding to the $\pm 1-\sigma$ extrema in the estimated uncertainty. We compare our $T_{\rm eff}$ and log(g) values and associated uncertainties to these tracks to estimate the age of KELT-3. These intersect the evolutionary track around 3.0 ± 0.2 Gyr.

To check that the isochrone age is consistent with the other parameters of KELT-3, we calculate the rotation period of the star, using the projected rotational velocity from §3.1 and the stellar radius from the full EXOFAST analysis in §3.5. Based on that rotation period of $P_{rot} / \sin i_{rot} = 7.11 \pm 0.54$ days, and the colors of the star, we calculate the maximum predicted age (subject to the inclination of the rotation axis to our line of sight) from the models of Barnes (2007), which comes to 2.3 ± 0.7 Gyr, which is fully consistent with the isochrone age. We also checked the KELT light curve for periodic variability associated with spot modulation as an independent measure of P_{rot}, but we were unable to detect any significant sinusoidal variability beyond the photometric noise.

3.4. *Characterizing the Faint Neighbor SDSS7J095434*

Although SDSS7J095434 is identified in the SDSS catalog, its proximity to the much brighter KELT-3 means that the SDSS catalog magnitudes are unreliable, necessitating the new photometric measurements we obtained for this star listed in §2.4. Based on those measurements and the flux ratios in §2.5, we are able to construct an SED for SDSS7J095434 (Figure 9). We follow the same procedure described in §3.2. Since we do not have independent measures of $T_{\rm eff}$, log(g), and [Fe/H], in this case we let those
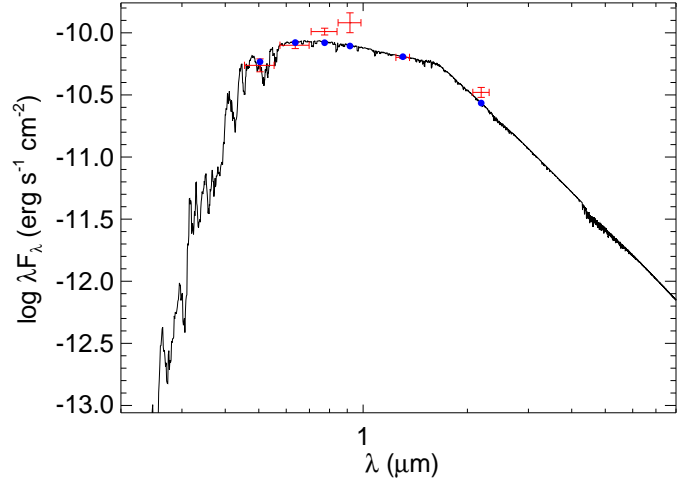

FIG. 9.— SED fit for SDSS7J095434, similar to Figure 6. The red errorbars indicate measurements of the flux of SDSS7J095434 listed in §2.4 and §2.5. The vertical errorbar indicates the photometric uncertainty, whereas the horizontal errorbar indicates the effective width of the passband. The solid curve is the best-fit theoretical SED from the NextGen models of Hauschildt et al. (1999). The blue dots are the predicted passband-integrated fluxes of the best-fit theoretical SED.

three parameters vary, along with A_V and d, although we limit the maximal value of A_V to 0.04 mag, which is the line-of-sight value based on the dust maps in Schlegel et al. (1998). The colors of SDSS7J095434 suggest it is a K3 star with $T_{\rm eff} = 4800 \pm 400$K, and $A_V = 0.02 \pm 0.02$. The corresponding distance for such a star with the observed apparent magnitude, assuming it is a dwarf, is 265^{+47}_{-40} pc, compared to a distance of 178 ± 16 pc for KELT-3. If SDSS7J095434 is rather a subgiant or giant star, it is located at a much further distance and thus certainly unassociated with KELT-3. Although the calculated distances to SDSS7J095434 and KELT-3 do not agree to within the quoted 1σ uncertainties, it is nevertheless possible (and perhaps likely) that they are associated. Assuming that the uncertainties in the distances are Gaussian distributed, we find that the inferred distances are consistent at the 1.76% level, assuming SDSS7J095434 is a dwarf star. Furthermore, as we argued above, it is likely that the uncertainties in the distances are underestimated.

3.5. *EXOFAST Analysis*

To determine the final orbital and physical parameters of the KELT-3 system, we use the results from the spectroscopic and SED analyses, the light curves, and the RVs of KELT-3 as inputs to EXOFAST (Eastman et al. 2013), which does a simultaneous Markov Chain Monte Carlo (MCMC) analysis of the entire system, including constraints on the stellar parameters M_* and R_* from the empirical relations in Torres et al. (2010). This method is similar to that described in detail in Siverd et al. (2012), but we note a few differences below.[26]

We scale the errors on the RV data such that the probability that the χ^2 was larger than the value we achieved, P(χ^2)

---

[26] In the EXOFAST analysis, which includes the modelling of the filter-specific limb darkening parameters of the transit, we employ the transmission curves defined for the primed SDSS filters rather than the unprimed versions. We expect any differences due to that discrepancy to be well below the precision of all our observations in this paper and of the limb darkening tables from Claret & Bloemen (2011).

was 0.5 so as to ensure the resulting parameter uncertainties were roughly accurate. We must do that process separately for the TRES and FIES RV observations, and since there are not enough observations from FIES or EXPERT to perform an independent fit, we fit the TRES data independently, scale their errors so $P(\chi^2) = 0.5$, then iteratively scale the FIES errors until the combined $P(\chi^2) = 0.5$, and repeat the same process for the EXPERT data. In addition, one of the TRES RVs was taken during the expected time of transit, and we therefore discarded that point so as not to be biased by the Rossiter-McLaughlin effect.

In this analysis, a complication arises because the light from KELT-3 and SDSS7J095434 was blended in all light curves except those from FTN. As in our analysis of KELT-2Ab (Beatty et al. 2012), which describes the process in more detail, we iteratively used the primary properties inferred from the full EXOFAST fit, combined with the model SED of the neighbor, to model and subtract the contribution of the flux from the neighbor in all the blended light curves.

The stellar and planetary parameters derived from this procedure are shown in Table 3. We see no evidence for a significant slope in the RV data – leaving the RV slope as a parameter to fit in the EXOFAST analysis yields a slope of -0.05 ± 0.36 m s^{-1} day^{-1}. The long baseline of the combined data sets does not constrain the slope as much as one might naively think. Since separate zero points are fit for each data set, the covariance between these zero points and slope is large, but it is taken into account in our stated uncertainty of the slope, which accounts for a drift in center of mass velocity with time. However, in our final analysis, when we fixed the slope to zero we assume no drift of the center of mass with time, and the entries for gamma in Table 3 are only relative values on an arbitrary scale. After recomputing the fit with the slope fixed to zero, we find a non-zero eccentricity that is apparently significant at the ~ 2–σ level, given the formal uncertainty on the eccentricity. However, as pointed out by Lucy & Sweeney (1971), there is a bias for small inferred values of the eccentricity, due to the fact that e is a positive definite quantity. Therefore, the true significance of a non-zero eccentricity is typically lower than one would infer based on the formal error and assuming a normal distribution. In this case, the fact that the values of $e\cos\omega_*$ and $e\sin\omega_*$ are both nearly consistent with zero suggests that the inferred non-zero eccentricity is indeed not significant. To further test the believably of the eccentricity, we performed a prayer bead analysis on the TRES data. We chose 100,000 random links from the eccentricity-fit Markov chain. We subtracted the corresponding model from our data, randomly permuted the epochs of residuals using a cyclical boundary, added the residuals back to a model with the same orbital parameters, but with the eccentricity set to zero, and then refit this artificial data set, allowing for eccentricity. Of these fits, 31.5% preferred an eccentricity of at least the value we measured in the original data set of 0.202, further suggesting this is an artifact of Lucy-Sweeney bias, the observed times, and red noise in residuals rather than a real, non-zero eccentricity. We therefore compute a second EXOFAST fit in which both the orbital eccentricity and the RV slope are fixed to zero, which we prefer, although we quote both fits for completeness.

Using the circular fit with no slope, our final uncertainty scalings are: 1.24 for the TRES RV data, 0.99 for the FIES RV data, and 1.20 for the EXPERT RV data. The RMS of the RV residuals of the fit to these scaled data are: 20.2 m s^{-1} for

TRES, 22.7 m s^{-1} for FIES, and 18.3 m s^{-1} for EXPERT. We also compute the RMS of the bisectors for the TRES and FIES spectra, obtaining an RMS of 14.3 m s^{-1} for the TRES data, and an RMS of 10.6 m s^{-1} for the FIES data. As noted previously, we did not measure bisectors for the EXPERT data.

We investigate the residuals of the circular fit for any signs of transit time variations (TTVs). When we fit the transits shown in Table 4, the constraints on T_C and P only come from the RV and the prior imposed from the KELT discovery data, not the follow up light curves. Using the transit times to constrain the period during the fit would artificially reduce any observed TTV signal. We fit a straight line to all mid transit times, listed in Table 4 and plotted in Figure 10, to derive a separate ephemeris from only the transit data: $T_0 = 2456034.29537 \pm 0.00038$, $P = 2.703418 \pm 0.000065$, with a χ^2 of 24.96 and 5 degrees of freedom. While the χ^2 is much larger than one would naively expect, this is largely dominated by the three transits at epoch -5, and in particular the FLWO transit, which is highly discrepant with the other two. We performed two tests to ensure that the large transit time offsets were not due to problems with the timestamps (e.g., (Eastman et al. 2010)). First, we have carefully checked that all quoted times are in BJD$_{TDB}$, re-deriving times from each observer directly from the data in the image headers. Second, we checked the accuracy of the observatory clocks, and found these to be good to at least 1 second, although these tests were done long after the observations analyzed here were taken. Therefore, we find no good reason to suspect a problem with the timestamps of the data. The transits shown in Figure 3 do not seem dominated by red noise, so it is worrisome that we could find such a large discrepancy (nearly 7 minutes or 4–σ) in the transit times at the same epoch. Regardless of the cause, it must be terrestrial in nature, so we conclude there is no convincing evidence for TTVs.

The final system parameters found for KELT-3, based on the circular, no-slope fit, are $M_* = 1.278^{+0.063}_{-0.061}M_\odot$, $R_* = 1.472^{+0.065}_{-0.067}R_\odot$, $T_{\rm eff} = 6306^{+50}_{-49}$ K, $\log(g) = 4.209^{+0.033}_{-0.031}$, and [Fe/H] $= 0.044^{+0.080}_{-0.082}$ The planet is an inflated hot Jupiter with $M_P = 1.477^{+0.066}_{-0.067}M_J$, and $R_P = 1.345 \pm 0.072R_J$, It is strongly irradiated, with an equilibrium temperature of $T_{\rm eq} = 1816^{+37}_{-39}$ K and an incident flux of $2.47^{+0.21}_{-0.20} \times 10^9$ erg s^{-1} cm^{-2}. The radius is about 25% larger than predicted from the models of Baraffe et al. (2008) for an irradiated planet with a mass of 1 to 2 M_J at 3 Gyr and a small amount of metals.

4. BACKTRACKING THE EVOLUTION OF KELT-3

KELT-3b is somewhat inflated, with a density of $0.75^{+0.12}_{-0.10}$ g cm^{-3}. In an investigation of transiting giant exoplanets, Demory & Seager (2011) found that exoplanets that are insolated beyond a certain threshold (2×10^8 erg s^{-1} cm^{-2}) have radii that are inflated compared to those planets with lower levels of insolation. KELT-3b falls well above that threshold, and follows the insolation-inflation trend displayed in Figure 1 of Demory & Seager (2011). It is worth investigating, however, whether that relationship has always held true. That is, has KELT-3b always been as insolated as it is now? If it turns out that KELT-3b only recently began receiving enhanced irradiation, this could provide an empirical probe of the timescale of inflation mechinisms (see Assef et al. (2009) and Spiegel & Madhusudhan (2012)).

In order to answer that question, we simulate the reverse-evolution of the star-planet system, using the measured pa-
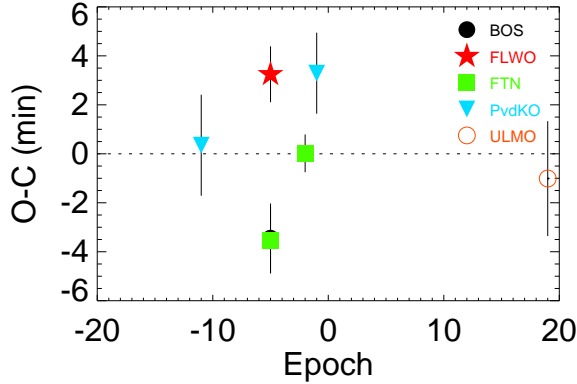
FIG. 10.— The residuals of the transit times from the best-fit ephemeris. The transit times are given in Table 4. The BOS observation at Epoch -5 is hidden behind the FTN observation at the same Epoch.

rameters listed in this paper as the present boundary conditions. This analysis is not intended to examine circularization of the planet, tidal locking to the star, or any type of planet-planet or planet-disk migration. Rather, it is a way to investigate the change in insolation of the planet over time due to the changing luminosity of the star and changing star-planet separation.

We include the evolution of the star, assumed to follow the YREC $1.3M_\odot$ model with solar metallicity (Siess et al. 2000). We assume that the stellar rotation was influenced only by tidal torques due to the planet, with no magnetic wind and treating the star like a solid body. We also assume a circular orbit throughout the full analysis. The results of our simulations are shown in Figure 11. We tested a range of values for the tidal quality factor of the star $Q_\star$, from $\log(Q_\star) = 5$ to $\log(Q_\star) = 9$. We find that although for certain values of $Q_\star$ the planet has moved substantially closer to its host during the past Gyr, in all cases the planet has always received more than enough flux from its host to keep the planet irradiated beyond the insolation threshold identified by Demory & Seager (2011). The rapid changes in semimajor axis and incident flux moving toward the future are mainly due to certain $Q_\star$ values being unphysically low and the logarithmic layout of the plots in age, and should not be taken as a sign that we are seeing the system at an especially unique moment of evolution.

5. DISCUSSION

KELT-3b is a typical hot Jupiter. Its host star is among the 20 brightest transiting planet hosts, and so the system provides an opportunity for detailed follow-up observations and analysis. Figure 12 shows the location of KELT-3 in a plot of host star brightness versus transit depth relative to other bright transiting planets hosts, demonstrating the potential value of this system for follow-up studies of its atmosphere.

Aside from its follow-up value as an especially bright transiting planet host, KELT-3 itself is nearly identical to the transiting planet host star HAT-P-2 (Pál et al. 2010). Both stars have the same masses, radii, effective temperatures, and surface gravities to within the measurement errors for both stars, and metallicities that differ by only 0.1 dex. The only stellar parameter that differs markedly is the rotational velocity, with HAT-P-2 rotating twice as fast as KELT-3 (20.8 km s^{-1} versus 10.2 km s^{-1}). The availability of such similar planet hosts can be used to compare different planet formation and evolution theories by comparing how closely exoplanet prop-
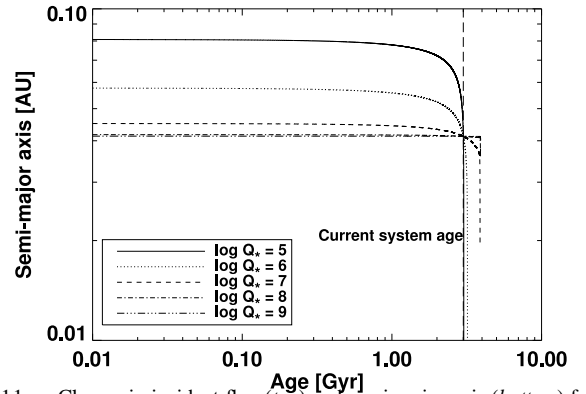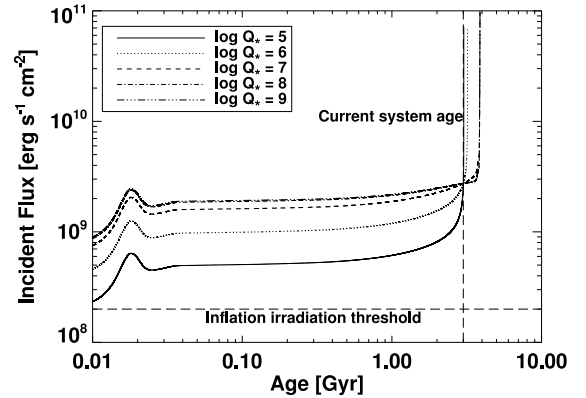
FIG. 11.— Change in incident flux (*top*) and semi-major axis (*bottom*) for KELT-3b, with different test values for $Q_\star$ for KELT-3. In all cases the planet has always received more than enough flux from its host to keep the planet irradiated beyond the insolation threshold of 2×10^8 erg s^{-1} cm^{-2} identified by Demory & Seager (2011).

erties track the properties of their host stars. This particular case offers an especially interesting comparison, since KELT-3b is a relatively typical hot Jupiter, while HAT-P-2b is quite an odd planet companion, with an exceptionally high mass (about $9M_J$) and eccentricity (0.52).

FIG. 12.— Transit depth as a function of the apparent V magnitude of the host star for a sample of transiting systems. KELT-3b is shown as the blue 3-pointed star. All else being equal, objects in the top left provide the best targets for follow-up. The other discoveries from the KELT survey, KELT-1b and KELT-2Ab, are also shown.

REFERENCES

Adelman-McCarthy, J. K., & et al. 2009, VizieR Online Data Catalog, 2294, 0
Alard, C. 2000, A&AS, 144, 363
Alard, C., & Lupton, R. H. 1998, ApJ, 503, 325
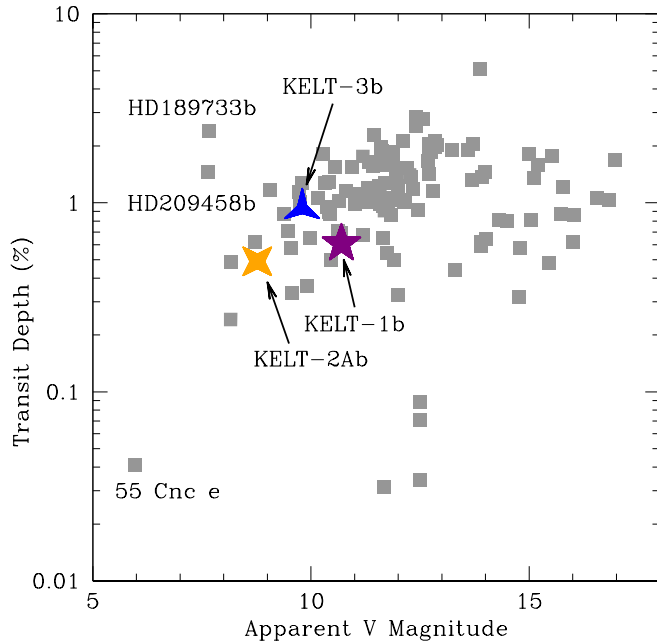Alonso, R., Brown, T. M., Torres, G., et al. 2004, ApJ, 613, L153
Alsubai, K. A., Parley, N. R., Bramich, D. M., et al. 2011, MNRAS, 417, 709
Assef, R. J., Gaudi, B. S., & Stanek, K. Z. 2009, ApJ, 701, 1616
Baglin, A. 2003, Advances in Space Research, 31, 345
Bakos, G. Á., Noyes, R. W., Kovács, G., et al. 2007, ApJ, 656, 552
Baraffe, I., Chabrier, G., & Barman, T. 2008, A&A, 482, 315
Barnes, S. A. 2007, ApJ, 669, 1167
Beatty, T. G., Pepper, J., Siverd, R. J., et al. 2012, arXiv:1206.1592
Bertin, E., & Arnouts, S. 1996, A&AS, 117, 393
Borucki, W. J., Koch, D., Basri, G., et al. 2010, Science, 327, 977
Buchhave, L. A., Bakos, G. Á., Hartman, J. D., et al. 2010, ApJ, 720, 1118
Buchhave, L. A., Latham, D. W., Johansen, A., et al. 2012, Nature, 486, 375
Carter, J. A., Winn, J. N., Holman, M. J., et al. 2011, ApJ, 730, 82
Claret, A., & Bloemen, S. 2011, A&A, 529, A75
Collier Cameron, A., Bouchy, F., Hébrard, G., et al. 2007, MNRAS, 375, 951
Collier Cameron, A., Wilson, D. M., West, R. G., et al. 2007, MNRAS, 380, 1230
Copenhagen University, O., Institute, A. O., Cambridge, Uk, & Real Instituto Y Observatorio de La Armada, F. E. S. 2006, VizieR Online Data Catalog, 1304, 0
Cutri, R. M., Skrutskie, M. F., van Dyk, S., et al. 2003, VizieR Online Data Catalog, 2246, 0
Cutri, R. M., & et al. 2012, VizieR Online Data Catalog, 2311, 0
Demarque, P., Woo, J.-H., Kim, Y.-C., & Yi, S. K. 2004, ApJS, 155, 667
Demory, B.-O., & Seager, S. 2011, ApJS, 197, 12
Dhital, S., West, A. A., Stassun, K. G., & Bochanski, J. J. 2010, AJ, 139, 2566
Djupvik, A. A., & Andersen, J. 2010, in "Highlights of Spanish Astrophysics V" eds. J. M. Diego, L. J. Goicoechea, J. I. González-Serrano, & J. Gorgas (Springer: Berlin), p. 211
Eastman, J., Siverd, R., & Gaudi, B. S. 2010, PASP, 122, 935
Eastman, J., Gaudi, B. S., & Agol, E. 2013, PASP, 125, 83

Fares, R., Donati, J.-F., Moutou, C., et al. 2012, MNRAS, 423, 1006
Fűrész, G. 2008, PhD thesis, Univ. Szeged
Ge, J., Zhao, B., Groot, J., et al. 2010, Proc. SPIE, 7735,
Gil de Paz, A., Boissier, S., Madore, B. F., et al. 2007, ApJS, 173, 185
Gil de Paz, A., Boissier, S., Madore, B. F., et al. 2009, VizieR Online Data Catalog, 217, 30185
Gould, A., & Morgan, C. W. 2003, ApJ, 585, 1056
Hartman, J. D., Gaudi, B. S., Holman, M. J., et al. 2008, ApJ, 675, 1254
Hauschildt, P. H., Allard, F., Ferguson, J., Baron, E., & Alexander, D. R. 1999, ApJ, 525, 871
Høg, E., Fabricius, C., Makarov, V. V., et al. 2000, A&A, 355, L27
Kovács, G., Zucker, S., & Mazeh, T. 2002, A&A, 391, 369
Kovács, G., Bakos, G., & Noyes, R. W. 2005, MNRAS, 356, 557
Kupka, F. G., Ryabchikova, T. A., Piskunov, N. E., Stempels, H. C., & Weiss, W. W. 2000, Baltic Astronomy, 9, 590
Kurucz, R. L. 1992, The Stellar Populations of Galaxies, 149, 225
Lucy, L. B., & Sweeney, M. A. 1971, AJ, 76, 544
Martin, D. C., Fanson, J., Schiminovich, D., et al. 2005, ApJ, 619, L1
McCullough, P. R., Stys, J. E., Valenti, J. A., et al. 2006, ApJ, 648, 1228
Pál, A., Bakos, G. Á., Torres, G., et al. 2010, MNRAS, 401, 2665
Pepper, J., Pogge, R. W., DePoy, D. L., et al. 2007, PASP, 119, 923
Richmond, M. W., Droege, T. F., Gombert, G., et al. 2000, PASP, 112, 397
Schlegel, D. J., Finkbeiner, D. P., & Davis, M. 1998, ApJ, 500, 525
Schneider, J., Dedieu, C., Le Sidaner, P., Savalle, R., & Zolotukhin, I. 2011, A&A, 532, A79
Siess, L., Dufour, E., & Forestini, M. 2000, A&A, 358, 593
Siverd, R. J., Beatty, T. G., Pepper, J., et al. 2012, ApJ, 761, 123
Skrutskie, M. F., Cutri, R. M., Stiening, R., et al. 2006, AJ, 131, 1163
Spiegel, D. S., & Madhusudhan, N. 2012, ApJ, 756, 132
Stetson, P. B. 1987, PASP, 99, 191
Torres, G., Andersen, J., & Giménez, A. 2010, A&A Rev., 18, 67
Valenti, J. A., & Piskunov, N. 1996, A&AS, 118, 595
Valenti, J. A., & Fischer, D. A. 2005, ApJS, 159, 141
Wang, J. PhD Thesis, University of Florida 2012
Wright, E. L., Eisenhardt, P. R. M., Mainzer, A. K., et al. 2010, AJ, 140, 1868
Wright, J. T., Marcy, G. W., Howard, A. W., et al. 2012, ApJ, 753, 160

TABLE 2
STELLAR PROPERTIES OF KELT-3

Parameter	Description (Units)	Value	Source	Reference
Names		BD+41 2024		
		TYC 2996-683-1		
		2MASS J09543439+4023170		
		GSC 02996-00683		
		SAO 43097		
α_{J2000}		09 54 34.391	Tycho-2	1
δ_{J2000}		+40 23 16.98	Tycho-2	1
FUV_{GALEX}		17.95 ± 0.14	GALEX	2
NUV_{GALEX}		14.09 ± 0.01	GALEX	2
B_T		10.397 ± 0.032	Tycho-2	1
V_T		9.873 ± 0.029	Tycho-2	1
r_{SDSS}		9.728 ± 0.015	Carlsberg	3
I_C		9.263 ± 0.057	TASS	4
J		8.963 ± 0.019	2MASS	5
H		8.728 ± 0.019	2MASS	5
WISE1		11.26 ± 0.022	WISE	6
WISE2		11.923 ± 0.019	WISE	6
WISE3		13.874 ± 0.023	WISE	6
WISE4		14.918 ± 0.227	WISE	6
μ_α	Proper Motion in RA (mas yr^{-1})	-28.9 ± 0.6	NOMAD	7
μ_δ	Proper Motion in Dec (mas yr^{-1})	-25.1 ± 0.7	NOMAD	7
U[a]	km s^{-1}	-25.6 ± 1.6	This paper	
V	km s^{-1}	-11.0 ± 2.2	This paper	
W	km s^{-1}	14.6 ± 1.3	This paper	
d	Distance (pc)	178 ± 16	This paper	
	Age (Gyr)	3.0 ± 0.2	This paper	
A_V	Visual Extinction	0.02 ± 0.02	This paper	

REFERENCES. — 1=Høg et al. (2000); 2=Martin et al. (2005); 3=Copenhagen University et al. (2006); 4=Richmond et al. (2000); 5=Cutri et al. (2003); Skrutskie et al. (2006); 6=Wright et al. (2010); Cutri et al. (2012); 7=Zacharias et al. (2004)

[a] Positive U is in the direction of the Galactic Center.

Zacharias, N., Monet, D. G., Levine, S. E., et al. 2004, Bulletin of the American Astronomical Society, 36, 1418

TABLE 3
MEDIAN VALUES AND 68% CONFIDENCE INTERVALS FOR THE PHYSICAL AND ORBITAL PARAMETERS
OF THE KELT-3 SYSTEM

Parameter	Units	Value; $e \neq 0$	Value; $e \equiv 0$, adopted
Stellar Parameters:			
M_*	Mass ($M_\odot$).........................	$1.277^{+0.063}_{-0.062}$	$1.278^{+0.063}_{-0.061}$
R_*	Radius ($R_\odot$).........................	$1.464^{+0.076}_{-0.077}$	$1.472^{+0.065}_{-0.067}$
L_*	Luminosity ($L_\odot$)....................	$3.04^{+0.35}_{-0.33}$	$3.08^{+0.31}_{-0.30}$
ρ_*	Density (cgs).........................	$0.574^{+0.086}_{-0.070}$	$0.565^{+0.071}_{-0.059}$
$\log g_*$ ...	Surface gravity (cgs).................	$4.213^{+0.039}_{-0.036}$	$4.209^{+0.033}_{-0.031}$
T_{eff}	Effective temperature (K)	6304 ± 50	6306^{+50}_{-49}
$[\mathrm{Fe/H}]$ ..	Metallicity..........................	0.046 ± 0.080	$0.044^{+0.080}_{-0.082}$
Planetary Parameters:			
e	Eccentricity.........................	$0.202^{+0.079}_{-0.089}$	$\equiv 0$
ω_*	Argument of periastron (degrees)	-158^{+48}_{-58}	$\equiv 90$
P	Period (days)........................	2.7033902 ± 0.0000099	$2.7033904^{+0.0000099}_{-0.0000100}$
a	Semi-major axis (AU)................	0.04120 ± 0.00067	$0.04122^{+0.00066}_{-0.00067}$
M_P	Mass (M_J)..........................	$1.444^{+0.069}_{-0.068}$	$1.477^{+0.066}_{-0.064}$
R_P	Radius (R_J).........................	1.340 ± 0.080	1.345 ± 0.072
ρ_P	Density (cgs)........................	$0.75^{+0.14}_{-0.11}$	$0.75^{+0.12}_{-0.10}$
$\log g_P$ ...	Surface gravity.......................	$3.300^{+0.047}_{-0.045}$	$3.306^{+0.044}_{-0.041}$
T_{eq}	Equilibrium temperature (K)..........	1811^{+43}_{-44}	1816^{+37}_{-39}
Θ	Safronov number.....................	$0.0696^{+0.0046}_{-0.0043}$	$0.0708^{+0.0045}_{-0.0040}$
$\langle F \rangle$	Incident flux (10^9 erg s^{-1} cm^{-2}).......	2.35 ± 0.25	$2.47^{+0.21}_{-0.20}$
RV Parameters:			
T_C	Time of inferior conjunction (BJD$_{\mathrm{TDB}}$)	$2456023.482^{+0.039}_{-0.031}$	2456023.459 ± 0.017
T_P	Time of periastron (BJD$_{\mathrm{TDB}}$)	$2456024.12^{+0.40}_{-0.42}$	—
K	RV semi-amplitude (m/s).............	182.3 ± 5.2	182.0 ± 5.2
$M_P \sin i$ ..	Minimum mass (M_J)	$1.437^{+0.068}_{-0.067}$	$1.470^{+0.065}_{-0.064}$
M_P/M_* .	Mass ratio	0.001081 ± 0.000040	0.001104 ± 0.000036
u	RM linear limb darkening	$0.6017^{+0.0056}_{-0.0054}$	$0.6014^{+0.0056}_{-0.0054}$
γ_{EXPERT} ·	m/s	-168^{+19}_{-20}	-170 ± 15
γ_{FIES}	m/s	$-47.5^{+8.1}_{-8.3}$	$-47.1^{+8.4}_{-8.3}$
γ_{TRES} ···	m/s	$-155.7^{+5.8}_{-5.7}$	-158.7 ± 4.9
$e \cos \omega_*$.	....	$-0.145^{+0.15}_{-0.100}$	—
$e \sin \omega_*$ ..	....	$-0.06^{+0.13}_{-0.11}$	—
$f(m1, m2)$	Mass function (M_J)...................	$0.00000166^{+0.00000017}_{-0.00000016}$	$0.00000177^{+0.00000016}_{-0.00000015}$
Primary Transit Parameters:			
R_P/R_* ..	Radius of the planet in stellar radii	0.0941 ± 0.0011	0.0939 ± 0.0011
a/R_*	Semi-major axis in stellar radii........	$6.05^{+0.29}_{-0.26}$	$6.02^{+0.24}_{-0.22}$
i	Inclination (degrees).................	$84.25^{+0.67}_{-0.64}$	$84.23^{+0.65}_{-0.58}$
b	Impact parameter.....................	0.612 ± 0.072	$0.606^{+0.037}_{-0.046}$
δ	Transit depth........................	0.00885 ± 0.00021	0.00882 ± 0.00021
T_{FWHM} ..	FWHM duration (days)	$0.1159^{+0.0040}_{-0.0051}$	$0.11414^{+0.00080}_{-0.00081}$
τ	Ingress/egress duration (days)	$0.0178^{+0.0037}_{-0.0029}$	0.0172 ± 0.0015
T_{14}	Total duration (days).................	$0.1346^{+0.0062}_{-0.0086}$	0.1313 ± 0.0016
P_T	A priori non-grazing transit probability	$0.147^{+0.024}_{-0.019}$	$0.1504^{+0.0055}_{-0.0057}$
$P_{T,G}$	A priori transit probablity	$0.178^{+0.029}_{-0.023}$	$0.1816^{+0.0069}_{-0.0072}$
$u_{1Sloang}$ ..	Linear Limb-darkening	$0.4675^{+0.0097}_{-0.0089}$	$0.4672^{+0.0098}_{-0.0089}$
$u_{2Sloang}$ ..	Quadratic Limb-darkening	$0.2748^{+0.0044}_{-0.0050}$	$0.2749^{+0.0044}_{-0.0050}$
$u_{1Sloani}$ ..	Linear Limb-darkening	$0.2347^{+0.0053}_{-0.0050}$	$0.2344^{+0.0053}_{-0.0051}$
$u_{2Sloani}$ ..	Quadratic Limb-darkening	$0.3103^{+0.0026}_{-0.0025}$	$0.3104^{+0.0026}_{-0.0025}$
$u_{1Sloanr}$ ..	Linear Limb-darkening	$0.3083^{+0.0064}_{-0.0059}$	$0.3080^{+0.0064}_{-0.0059}$
$u_{2Sloanr}$ ..	Quadratic Limb-darkening	$0.3195^{+0.0021}_{-0.0020}$	$0.3196^{+0.0022}_{-0.0020}$
$u_{1Sloanz}$ ..	Linear Limb-darkening	$0.1835^{+0.0048}_{-0.0046}$	0.1833 ± 0.0047
$u_{2Sloanz}$ ..	Quadratic Limb-darkening	$0.3016^{+0.0020}_{-0.0025}$	$0.3016^{+0.0021}_{-0.0025}$
Secondary Eclipse Parameters:			
T_S	Time of eclipse (BJD$_{\mathrm{TDB}}$)	$2456024.58^{+0.23}_{-0.13}$	2456022.107 ± 0.017
b_S	Impact parameter.....................	$0.551^{+0.10}_{-0.086}$	—
$T_{S,FWHM}$ ·	FWHM duration (days)	$0.1107^{+0.0064}_{-0.0093}$	—
τ_S	Ingress/egress duration (days)	$0.0152^{+0.0046}_{-0.0029}$	—
$T_{S,14}$	Total duration (days).................	$0.126^{+0.011}_{-0.012}$	—
P_S	A priori non-grazing eclipse probability	$0.164^{+0.019}_{-0.020}$	—
$P_{S,G}$	A priori eclipse probability	$0.198^{+0.023}_{-0.024}$	—

TABLE 4
Transit Times for KELT-3

Telescope and filter	Epoch	T_C (BJD$_{TDB}$)	Error (seconds)	O-C (seconds)	(O - C)/Error
PvdKO, f	-11	2456004.558023	123	21.02	0.17
BOS, g	-5	2456020.775891	84	-206.86	-2.44
FLWO, i	-5	2456020.780541	68	194.90	2.85
FTN, z	-5	2456020.775835	81	-211.70	-2.60
FTN, z	-2	2456028.888551	46	1.12	0.02
PvdKO, g	-1	2456031.594242	99	197.54	1.99
ULMO, r	19	2456085.659606	140	-60.60	-0.43